Use of NDVI and Land Surface Temperature for Drought Assessment: Merits and Limitations

ARNON KARNIELI,* NURIT AGAM,+ RACHEL T. PINKER,# MARTHA ANDERSON,+ MARC L. IMHOFF,@ GARIK G. GUTMAN,& NATALYA PANOV,* AND ALEXANDER GOLDBERG*

* *Remote Sensing Laboratory, Jacob Blaustein Institutes for Desert Research, Ben-Gurion University of the Negev, Sede Boqer, Israel*
+ *Hydrology and Remote Sensing Laboratory, ARS, USDA, Beltsville, Maryland*
# *Department of Atmospheric and Oceanic Science, University of Maryland, College Park, College Park, Maryland*
@ *Biospheric Sciences Branch, NASA Goddard Space Flight Center, Greenbelt, Maryland*
& *NASA Headquarters, Washington, D.C.*

(Manuscript received 23 October 2008, in final form 3 July 2009)

ABSTRACT

A large number of water- and climate-related applications, such as drought monitoring, are based on spaceborne-derived relationships between land surface temperature (LST) and the normalized difference vegetation index (NDVI). The majority of these applications rely on the existence of a negative slope between the two variables, as identified in site- and time-specific studies. The current paper investigates the generality of the LST–NDVI relationship over a wide range of moisture and climatic/radiation regimes encountered over the North American continent (up to 60°N) during the summer growing season (April–September). Information on LST and NDVI was obtained from long-term (21 years) datasets acquired with the Advanced Very High Resolution Radiometer (AVHRR). It was found that when water is the limiting factor for vegetation growth (the typical situation for low latitudes of the study area and during the midseason), the LST–NDVI correlation is negative. However, when energy is the limiting factor for vegetation growth (in higher latitudes and elevations, especially at the beginning of the growing season), a positive correlation exists between LST and NDVI. Multiple regression analysis revealed that during the beginning and the end of the growing season, solar radiation is the predominant factor driving the correlation between LST and NDVI, whereas other biophysical variables play a lesser role. Air temperature is the primary factor in midsummer. It is concluded that there is a need to use empirical LST–NDVI relationships with caution and to restrict their application to drought monitoring to areas and periods where negative correlations are observed, namely, to conditions when water—not energy—is the primary factor limiting vegetation growth.

1. Introduction

a. At issue

Periods of persistent abnormally dry weather, known as droughts, can produce a serious agricultural, ecological, or hydrological imbalance. Drought harshness depends upon the degree of moisture deficiency, duration, and the size of the affected area (Wilhite and Glantz 1985). The serious effects droughts have on human life and well-being have led to increasing efforts to develop and implement various quantitative measures of drought extent and severity.

Several drought indices utilize ground-based measurements: some indices are based on energy-balance models, whereas other indices use spaceborne data, either solely or in combination with energy-balance models (Heim 2002; Quiring and Papakryiakou 2003). Satellite-derived drought indices typically use observations in multispectral bands, each of which provides different information about surface conditions. Because droughts are naturally associated with vegetation state and cover, vegetation indices (VIs) are commonly used for this purpose (e.g., Tucker and Choudhury 1987), utilizing data in the visible red (R), near infrared (NIR), and the shortwave infrared bands. Some drought indices are based on observations in

Corresponding author address: Prof. Arnon Karnieli, Remote Sensing Laboratory, Jacob Blaustein Institutes for Desert Research, Ben-Gurion University of the Negev, Sede Boker Campus 84990, Israel.
E-mail: karnieli@bgu.ac.il

DOI: 10.1175/2009JCLI2900.1

the thermal infrared (TIR) spectral region, which conveys information about vegetation health and soil moisture status.

b. NDVI as an indicator of drought

The most commonly used VI is the normalized difference vegetation index (NDVI) [Eq. (1)], which is based on the difference between the maximum absorption of radiation in R as a result of chlorophyll pigments and the maximum reflectance in NIR spectral region as a result of leaf cellular structure (Tucker 1979):

$$\mathrm{NDVI} = \frac{(\rho_{\mathrm{NIR}} - \rho_R)}{(\rho_{\mathrm{NIR}} + \rho_R)}, \tag{1}$$

where ρ is reflectance in the respective spectral bands. The soil spectrum typically does not show such a distinct spectral difference between these bands, and thus the NDVI allows for separation of vegetation from the soil background.

Tucker and Choudhury (1987) found that NDVI could be used as a response variable to identify and quantify drought disturbance in semiarid and arid lands, with low values corresponding to stressed vegetation. More recently, Ji and Peters (2003) found that NDVI is an effective indicator of vegetation response to drought in the Great Plains of the United States, based on the relationships between NDVI and a meteorologically based drought index. The vegetation condition index [VCI; Eq. (2)] developed by Kogan (1995, 1997, 2002) normalizes NDVI on a pixel-by-pixel basis, scaling between minimum and maximum values of NDVI ($\mathrm{NDVI}_{\mathrm{min}}$ and $\mathrm{NDVI}_{\mathrm{max}}$, respectively), as observed at each pixel over a long temporal record since 1981:

$$\mathrm{VCI} = \frac{\mathrm{NDVI}' - \mathrm{NDVI}_{\mathrm{min}}}{\mathrm{NDVI}_{\mathrm{max}} - \mathrm{NDVI}_{\mathrm{min}}}, \tag{2}$$

where NDVI′ is the average NDVI over a composite period of interest (which can be a week, decade, month, growing season, or a year). The normalization serves to emphasize relative changes in the local NDVI signal through time while reducing the influence of spatial variability in NDVI phenology between different land cover types and climatic conditions.

c. LST as an indicator of drought

Land surface temperature (LST) derived from TIR band data has also been found to provide vital and useful information on the state of the land surface and is widely implemented in formulating the energy and water budgets at the surface–atmosphere interface (Gutman 1990). In this context, LST serves as a proxy for assessing evapotranspiration, vegetation water stress, soil moisture, and thermal inertia (Moran et al. 1994; Ottle and Vidalmadjar 1994; Moran et al. 1996; Sobrino et al. 1998; Gupta et al. 2002; Narasimhan et al. 2003; Jang et al. 2006; Anderson et al. 2007).

Recognizing that LST provides useful information about vegetation condition, Kogan (1995; 2000) adapted the VCI normalization approach [Eq. (2)] to LST and developed the temperature condition index (TCI) based on brightness temperature (BT) values:

$$\mathrm{TCI} = \frac{\mathrm{BT}_{\mathrm{max}} - \mathrm{BT}'}{\mathrm{BT}_{\mathrm{max}} - \mathrm{BT}_{\mathrm{min}}}, \tag{3}$$

where the BT′ is the average BT value for a composite period of interest, and $\mathrm{BT}_{\mathrm{max}}$ and $\mathrm{BT}_{\mathrm{min}}$ are pixel-specific long-term maximum and minimum temperatures identified over the period of record. Note that to apply the TCI for determining temperature-related vegetation stress, it is formulated as a reverse ratio to the VCI. Although the VCI increases with NDVI, the TCI decreases with LST based on the hypothesis that higher land surface temperatures indicate soil moisture deficiencies and therefore stress in the vegetation canopy (Kogan 1995, 2000).

d. LST–NDVI relationships as an indicator of drought

Both visible to near-infrared (VNIR) and TIR data have advantages and disadvantages in terms of utility for drought detection. Although LST-based assessments of land surface conditions have shown a better performance over sparse vegetation cover (Friedl and Davis 1994), VNIR-based indices are more reliable at assessing the condition and dynamics of vegetation over intermediate levels of vegetation cover (about 50%; Huete et al. 1985). Therefore, extensive work has been devoted to combining these state variables into a unified drought indicator, based on the assumption that complementary information in these wave bands may provide a more robust characterization for different phenomena at the land surface. Studies have revealed a strong negative correlation between NDVI and LST (Gurney et al. 1983; Goward et al. 1985; Hope et al. 1986; Hope 1988; Goward and Hope 1989; Nemani and Running 1989; Price 1990; Smith and Choudhury 1991; Hope and McDowell 1992; Nemani et al. 1993; Prihodko and Goward 1997; Goward et al. 2002), resulting from the cooling effects of canopy transpiration. These early studies were typically limited to relatively small areas and based on a limited number of images. The spatiotemporal variability of the LST–NDVI relationship on continental or global scales has been investigated in several studies (Schultz and Halpert 1995; Lambin and Ehrlich 1996; Churkina and Running 1998; Nemani et al. 2003; Julien et al. 2006; Olthof and

Latifovic 2007; Sun and Kafatos 2007; Julien and Sobrino 2009). However, all of these studies used only the yearly or growing season mean values.

Prior studies have assessed the variability in the slope of the inverse LST–NDVI relationship in association with local topographic and environmental conditions. Goward and Hope (1989), for example, stated that the LST–NDVI slope and intercept are expected to vary from day to day based on the magnitude of incident solar radiation, advective atmospheric conditions, and surface moisture availability. Simulations performed by Hope et al. (1988) revealed that soil moisture potential affects the relationship between canopy temperature and NDVI. Using a LST–NDVI scatterplot, Price (1990) differentiated between areas of full vegetation cover, dry soils, and moist soils. Hope and McDowell (1992) used the LST–NDVI relation to distinguish between burned and unburned surfaces. The LST–NDVI slope was also found to be related to vegetation type and topography as well as to vegetation cover (Nemani et al. 1993). Goward et al. (1994) showed that although a negative slope exists for sparse vegetation cover, the slope of a closed vegetation canopy is insignificant. Goetz (1997) showed that the slope varies with climatic conditions, with steeper slopes associated with drier situations.

The LST–NDVI slope has been used in numerous applications associated with water and energy balance. The slope was found to be related to moisture availability and canopy resistance, indicating vegetation stress and/or soil water stress (Nemani and Running 1989; Carlson et al. 1994; Gillies and Carlson 1995; Gillies et al. 1997; Goetz 1997). Nemani et al. (1993) found that the slope is inversely correlated to a crop moisture index. Other studies showed that the slope is related to the rate of evapotranspiration from the surface (Prihodko and Goward 1997; Boegh et al. 1999). Goward et al. (2002) used NDVI and LST data to predict near-surface air temperature. The typical ''triangle'' or ''trapezoidal'' distributions of image pixels in the NDVI–LST space have been used to model soil–vegetation–atmosphere interactions in terms of evaporation and evapotranspiration (Carlson et al. 1994; Moran et al. 1994; Gillies and Carlson 1995; Moran et al. 1996; Gillies et al. 1997; Sandholt et al. 2002; Jang et al. 2006; Stisen et al. 2007). Other applications include large-scale land cover classification, change detection, vegetation phenology, and evaluation of desertification and climate change processes (Achard and Blasco 1990; Lambin and Strahler 1994a,b; Lambin and Ehrlich 1995; Ehrlich and Lambin 1996; Lambin 1996; Lambin and Ehrlich 1996, 1997; Nemani and Running 1997; Sobrino and Raissouni 2000; Dall'Olmo and Karnieli 2002; Karnieli and Dall'Olmo 2003; Tateishi and Ebata 2004; Wan et al. 2004; Julien et al. 2006).

Considerable attention has been given to the inverse relation between LST and NDVI with respect to drought monitoring. During drought periods, NDVI at a given pixel will typically be relatively low, whereas LST is expected to be relatively high because of both vegetation deterioration and higher contribution of a soil signal (Kogan 2000). McVicar and Bierwirth (2001), for example, used a simple ratio between LST and NDVI to map drought. The vegetation health index (VHI) developed by Kogan (1995) combines two indicators of comparable magnitude, using the VCI and TCI described earlier [Eqs. (2) and (3)]:

$$\mathrm{VHI} = \alpha \mathrm{VCI} + (1 - \alpha)\mathrm{TCI}, \tag{4}$$

where α and $(1 - \alpha)$ define the relative contributions of each index. Because of the lack of more accurate information, α has been usually assigned a value of 0.5, assuming an equal contribution of both variables to the combined index (Kogan 2000). The VHI has been applied in a range of applications, such as drought detection, assessment of drought severity and duration, and early drought warning (Seiler et al. 1998); monitoring crop yield and production during the growing season (Unganai and Kogan 1998); vegetation density and biomass estimation (Gitelson et al. 1998); assessment of irrigated areas (Boken et al. 2004); and estimation of excessive wetness (in contrast to drought; Unganai and Kogan 1998). Such applications have been conducted in many parts of the world at various scales—from global (Kogan 1997, 2000, 2002) to regional (e.g., Liu and Kogan 1996) and local scales (e.g., Seiler et al. 1998). The VHI is a standard product for drought monitoring, provided weekly by the National Oceanic and Atmospheric Administration (NOAA; available online at http://www.orbit.nesdis.noaa.gov/smcd/ and http://lwf.ncdc.noaa.gov/oa/climate/research/dm/vhi.html) and other institutes (e.g., http://www.fe-lexikon.info/ and http://www.reliefweb.int/).

The validity of the VHI as a drought detection tool relies on the assumption that NDVI and LST at a given pixel will vary inversely over time, with variations in VCI and TCI driven by local moisture conditions. However, when examined over spatially expanded areas and long periods, the relationship between LST and NDVI is found to be nonunique and often nonnegative. Kawashima (1994) distinguished between urban and suburban sites and observed positive relationships on a clear winter night as a result of higher vegetation density in the suburban area than in the urban area. Lambin and Ehrlich (1996) worked on a continental scale in Africa and found positive correlations over an evergreen forest and negative correlations over drier biomes. A positive slope

was also shown for the native evergreen forests in southern Australia (Smith and Choudhury 1991). Karnieli et al. (2006) demonstrated that the slope of LST versus NDVI over Mongolia changes with respect to geobotanical regions and latitude. A negative slope was observed in the arid regions of southern Mongolia, whereas the slope was positive in the northern part of the country. Olthof and Latifovic (2007) showed that the NDVI of trees and shrubs in Canada correlates positively with LST, whereas Sun and Kafatos (2007) found that these correlations over the North American continent are season and time-of-day dependent. A positive correlation was found in winter, whereas strong negative correlations were found during the warm seasons. The global distribution of the LST and NDVI relations shows negative correlations over drylands and midlatitudes and positive correlations over the tropics and high latitudes (Schultz and Halpert 1995; Churkina and Running 1998; Nemani et al. 2003; Julien and Sobrino 2009).

In summary, positive relationships between LST and NDVI tend to develop in areas where vegetation growth is energy or temperature limited. Several studies confirmed via warming experiments in high-latitude regions that warming generally induces an increase in plant biomass, abundance, height, cover, and net primary productivity (NPP; Chapin et al. 1995; Graglia et al. 1997; Dormann and Woodin 2002; Van Wijk et al. 2003; Stow et al. 2004; Walker et al. 2006). In such areas, higher LST reflects conditions that are more conducive to plant development through various biochemical processes (Badeck et al. 2004). Increased LST also drives processes within the soil, such as microbial activity, nitrogen availability, and nutrient uptake (Nadelhoffer et al. 1991; Chapin et al. 1995). Therefore, in high latitudes, increasing LST should not be interpreted as a signal of vegetation stress.

e. Objectives

Diverse findings regarding the LST–NDVI relationship are reported in literature. In general, prior studies suggest that the sign of the LST–NDVI slope may be governed by whether vegetation growth is water limited (negative slope) or energy–temperature limited (positive slope). The latter condition is prevalent at high latitudes or in the evergreen tropical forests, whereas the former may occur at lower latitudes, especially in drylands (Nemani and Running 1989; Nemani et al. 1993; Lambin and Ehrlich 1996; Karnieli et al. 2006).

The objective of this paper is to investigate the generality of the LST–NDVI relationship with respect to drought monitoring and assessment. The study includes the wide range of moisture and climatic–radiation regimes encountered over the North American continent (up to 60°N) during the summer growing season (April–September) using long-term (21 years) datasets from the Advanced Very High Resolution Radiometer (AVHRR). Over this domain, it was hypothesized that the slope of LST versus NDVI increases with latitude, and that the sign of the slope is related to the locally prevalent factor limiting vegetation growth: energy versus moisture. The goal is to identify times and areas where simple empirical drought indices—such as the VHI, which assumes a negative slope between NDVI and LST—should work well and where their application may be problematic.

2. Data and methodology

A wide range of climatic and physical variables affects NDVI, LST, and the relationship between plant cover and temperature. The primary variables among these are solar radiation, air temperature close to the earth's surface, and rainfall (Churkina and Running 1998; Nemani et al. 2003). Radiation is important because photosynthesis occurs only in environments with a sufficient amount of light, and temperature determines photosynthetic and respiration rates as well as the amount of nutrients available for plant uptake through the influence on litter decomposition rate. Precipitation is crucial as the main source of water supply. Secondary biophysical variables of interest closely related to these primary climatic factors include soil moisture, evapotranspiration, and land cover extent and type. For critical examination of the NDVI–LST relationship, long-term information about such variables was assembled from surface and satellite sources and from numerical weather prediction models. The current study domain includes the United States and Canada (up to 60°N), where comprehensive ancillary data are available.

a. NDVI and LST data

A suitable spaceborne instrument for retrieving long-term NDVI and LST data is the AVHRR carried on the NOAA series of satellites. This instrument provides imagery in the visible *R*, NIR, and TIR spectral bands. Although originally designed for atmospheric and oceanic applications, the sensor has been widely used for land applications, particularly for assessing the state and temporal dynamics of vegetation at coarse spatial resolution (1.1 km) over regional-to-global scales. Availability of continuous global observations on a daily basis since June 1981 makes this sensor attractive for many long-term vegetation and climate change studies.

In this study, 21 years of NOAA-AVHRR data (July 1981–December 2001) from the NOAA/National Aeronautics and Space Administration (NASA) Pathfinder

AVHRR Land (PAL) dataset (available online at http://daac.gsfc.nasa.gov/interdisc/readmes/pal_ftp.shtml) are used. These data were obtained from the afternoon satellites—namely, *NOAA-7*, *NOAA-9*, *NOAA-11*, *NOAA-14*, and *NOAA-16*. Specifically, the AVHRR data used here include monthly composites of calibrated reflectances from bands 1 and 2, and brightness temperatures from bands 4 and 5 at 8-km resolution. Preprocessing of the PAL dataset included improved navigation, cloud masking, calibration, and Rayleigh atmospheric correction [Nemani et al. (2003) and supporting references and notes therein].

On the basis of the PAL dataset, NDVI values are computed using Eq. (1) with bands 1 and 2 as ρ_R and ρ_{NIR}, respectively. Brightness temperatures of bands 4 (BT_4) and 5 (BT_5) are used to compute LST utilizing a split-window algorithm (Coll et al. 1994; Jang et al. 2006):

$$\mathrm{LST} = \mathrm{BT}_4 + [1.29 + 0.28(\mathrm{BT}_4 - \mathrm{BT}_5)](\mathrm{BT}_4 - \mathrm{BT}_5) + 45(1 - \varepsilon_4) - 40\Delta\varepsilon, \quad (5)$$

where ε_4, the surface emissivity in band 4, is calculated as

$$\varepsilon_4 = 0.9897 + 0.029 \ln(\mathrm{NDVI}) \quad (6)$$

and the emissivity difference between bands 4 and 5 ($\Delta\varepsilon$) as

$$\Delta\varepsilon = 0.01019 + 0.01344 \ln(\mathrm{NDVI}). \quad (7)$$

Monthly LST and NDVI data over the study area were downloaded for a 6-month period (April–September) for each year. Pixels representing inland water bodies (NDVI $<$ 0 and LST $<$ 200 K) were excluded from the analysis. In addition, a small number of noisy pixels (mostly due to local registration artifacts) were eliminated from each image. The data were averaged for two months, representing subperiods of the vegetation growing season—the beginning (April–May), middle (June–July), and end (August–September). Long-term averages of NDVI and LST were also computed from the bimonthly values. In total, 1 long-term average field and 21 yearly images were derived for both NDVI and LST.

b. Primary variables

1) AIR TEMPERATURE

Gridded data of long-term monthly-mean air temperature at 2 m above ground were extracted from the National Centers for Environmental Prediction (NCEP) North American Regional Reanalysis (NARR) dataset (Mesinger et al. 2006; available online at http://www.cdc.noaa.gov/cdc/data.narr.monolevel.html). This version of NARR uses the Noah land surface model (LSM) embedded within the mesoscale Eta model (Ek et al. 2003). The grid resolution is approximately 0.3° (32 km).

2) RAINFALL

Gridded long-term averages of monthly precipitation for North America at 0.25° spatial resolution were obtained from monthly-mean values from NOAA's Climate Prediction Center (CPC) using gauge observations from 1948 to the present (available online at http://www.cpc.ncep.noaa.gov/products/global_precip/html/web.shtml), averaged to 0.5°. Similar data for Canada, at 1° resolution, were also used (J. Janowiak and W. Shi 2007, personal communication).

3) RADIATION

Under the International Satellite Cloud Climatology Project (ISCCP; Schiffer and Rossow 1985; Rossow and Schiffer 1999; Rossow and Dueñas 2004) time series of cloud cover and top-of-the-atmosphere radiances are produced from an amalgamation of observations from five geostationary satellites as well as from the AVHRR instrument on board the polar-orbiting satellites. Over the United States, most of the observations come from the Geostationary Operational Environmental Satellite (GOES) series of satellites. These observations are gridded at 2.5° spatial resolution at a time scale of three hours, and daily values are produced by integration from sunrise to sunset. The daily values are aggregated to monthly means as used in this study. The ISCCP cloud products (version D1) are used to produce surface radiative fluxes with the University of Maryland inference scheme originally described in Pinker and Ewing (1985) and Pinker and Laszlo (1992) and as modified in respect to the representation of aerosols (Liu et al. 2005; Liu and Pinker 2008; Liu et al. 2008), data merging techniques (Zhang et al. 2007), and elevation correction.

These radiative fluxes have been used in numerous studies (Sui et al. 2003; Rodriguez-Puebla et al. 2008) and are being evaluated in the Global Energy and Water Cycle Experiment (GEWEX) Radiative Flux Assessment framework (available online at http://eosweb.larc.nasa.gov/GEWEX-RFA/).

c. Secondary variables

1) SOIL MOISTURE AND EVAPOTRANSPIRATION

Soil moisture and evapotranspiration information was also obtained from the NCEP NARR reanalysis (Mesinger et al. 2006) at 32-km resolution. Soil moisture data from two layers were used—namely, average estimates for the uppermost 10 cm and the plant root zone

(0–200 cm). The 10-cm soil moisture is more closely related to surface temperature under low-vegetation cover conditions, whereas the deeper moisture content should better correlate under high-vegetation cover conditions.

2) FRACTIONAL VEGETATION COVER

Fractional vegetation cover was determined as follows (Choudhury et al. 1994):

$$f_c = 1 - \left(\frac{\mathrm{NDVI}_{\mathrm{scmax}} - \mathrm{NDVI}_i}{\mathrm{NDVI}_{\mathrm{scmax}} - \mathrm{NDVI}_{\mathrm{scmin}}} \right)^{0.625}, \qquad (8)$$

where $\mathrm{NDVI}_{\mathrm{scmax}}$ and $\mathrm{NDVI}_{\mathrm{scmin}}$ are the maximum and minimum NDVI values from the scene.

3) LAND COVER CLASSIFICATION

To investigate the relationship of NDVI–LST slope with cover type, a land cover classification was used consisting of 14 classes at 8-km pixel resolution based on AVHRR observations (Defries et al. 2000; Hansen et al. 2000; available online at http://glcf.umiacs.umd.edu/data/landcover/; Defries et al. 2000; Hansen et al. 2000). An independent land cover database generated from AVHRR observations over Canada and consisting of 12 classes is available (online at ftp://ftp.ccrs.nrcan.gc.ca/ad/NLCCLandCover/). In the current work, land cover classes were aggregated into six classes: 1) evergreen needleleaf forest (including mixed cover and woodland); 2) deciduous broadleaf forest; 3) crops; 4) grassland and shrubland (including wooded grassland, closed shrubland, and open shrubland); 5) low vegetation; and 6) bare soil. This classification follows the University of Maryland database except for the ''open shrubland'' class, which was split between ''low vegetation'' for northeast Canada and ''grassland and shrubland'' elsewhere. The ''evergreen broadleaf forest,'' ''deciduous broadleaf forest,'' and ''urban and built up'' classes were excluded from the analysis.

3. Analysis and discussion

a. Spatiotemporal relationships between LST and NDVI

In the triangle/trapezoid approach to assessing regional soil moisture availability, the LST–NDVI relationship is mapped over the spatial domain of interest. Following this approach, long-term (1981–2001) averages of NDVI and LST for each of three bimonthly subperiods—April–May, June–July, and August–September (Figs. 1a–f)—were used to create density scatterplots (Figs. 1g–i). In these plots, yellow and red colors represent higher concentrations of pixels. In each subperiod, two distinct populations can be identified: one with the typical negative slope, indicative of moisture-limited vegetation growth; and a second with a small positive slope, showing little variability in LST over a wide range in NDVI. To ascertain whether the slope of LST versus NDVI gradually varies with latitude (similar to the trend identified in Mongolia (Karnieli et al. 2006)), eight points along a north–south transect over the Great Plains were selected at approximately 5° intervals (Fig. 2). For each point, the April and May monthly LST and NDVI averages were extracted for each of the 21 years of available data, resulting in 42 data pairs (21 years times 2 months) per point (sufficient for statistical analysis). Figure 3 shows plots of LST versus NDVI for the eight points along the transect. As expected, the slope gradually increases from negative to positive from the south northward. Along this transect, only the two northern points (Figs. 3a,b) showed positive significant correlations; the correlations at the four central points (Figs. 3c–f) were found to be insignificant, and significant negative correlations are identified only at the two most southern points (Figs. 3g,h).

To study the spatial patterns of temporal correlations between LST and NDVI, the correlation coefficient r was computed for each pixel in the study area, stratified by subperiod (Figs. 4a–c). The blue areas show negative correlation coefficients, indicative of moisture-limited vegetation growth where the VHI may work well. The red areas have positive correlation and are likely energy limited, and the VHI may give confusing information. The white areas show insignificant correlation between LST and NDVI and therefore the application of the VHI is not suitable over this region.

Corresponding histograms of r values are shown in Figs. 4d–f to highlight variations in the distributions of positive and negative slopes between the seasons. In the April–May image (Fig. 4a), representing pre-emergence of vegetation over most of the domain, r is largely stratified by latitude. Positive r occurred in 60% of the entire domain and insignificant r in 25%. Only 15% of the domain, in the southernmost part of the study area, exhibits a significant negative correlation in the temporal behavior of NDVI and LST. This is also reflected in the frequency histograms where negative skewness ($\gamma = -0.79$) in r distribution was computed (Fig. 4d). In comparison, during June–July, 57% of the domain is characterized by negative correlation, whereas insignificant and positive correlations in 29% and 14%, respectively. Variation in r is less clearly characterized by latitude (Fig. 4b) and significant positive skewness in r ($\gamma = 0.35$) is found (Fig. 4e). Toward the end of the growing season (August–September), a north-to-south gradient reappears. The positive, insignificant, and negative correlations are almost evenly distributed—31%,

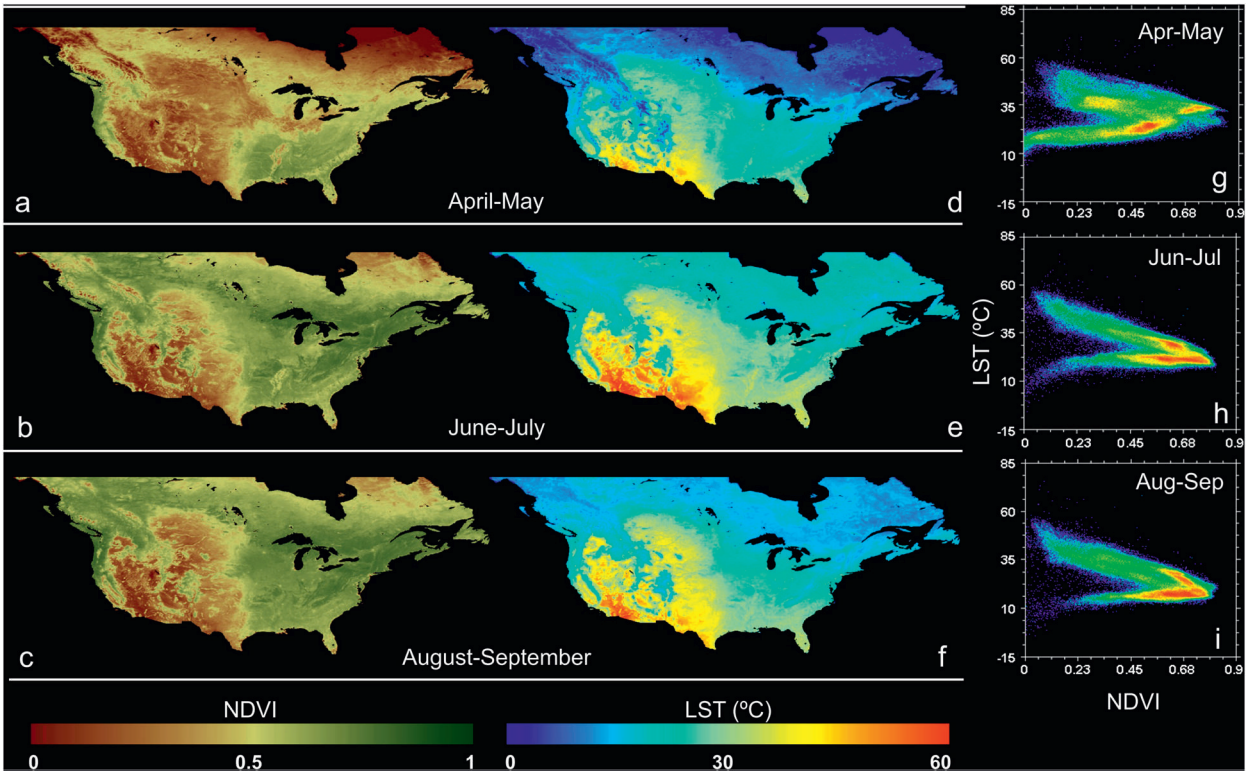

FIG. 1. Long-term averages of NDVI for the three subperiods of the growing seasons: (a) April–May, (b) June–July, and (c) August–September. (d)–(f) Long-term averages of LST and (g)–(i) density scatterplots of LST vs NDVI for the same subperiods. Note that in the density plots, in each subperiod, one branch of the correlation is negative while the other is positive or insignificant. Yellow and red colors represent higher concentration of pixels.

37%, and 32%, respectively—with a small positive skewness value ($\gamma = 0.13$, statistically significant) (Figs. 4c,f).

b. *Climatic factors driving LST–NDVI correlations*

The seasonal variability in the spatial distribution of the LST–NDVI correlation coefficient over the North American domain implies that different climatic variables govern the correlation at different times of the year. The apparent seasonal shifts between energy- and moisture-limited vegetation growth conditions suggest that solar radiation and near-surface (2 m) air temperature may be important factors in spring and fall, whereas

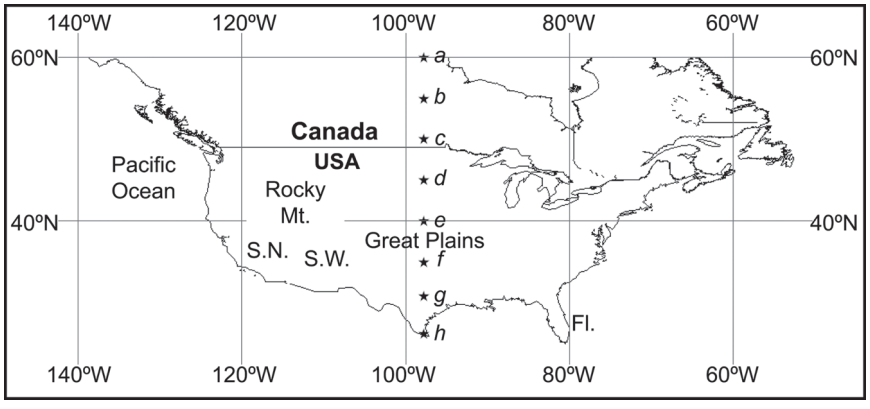

FIG. 2. Map of the study area. Stars mark locations along longitude 40°18′W where long-term (1981–2001) LST–NDVI relationships for April–May were examined (Fig. 4). Relevant geographic locations are marked.

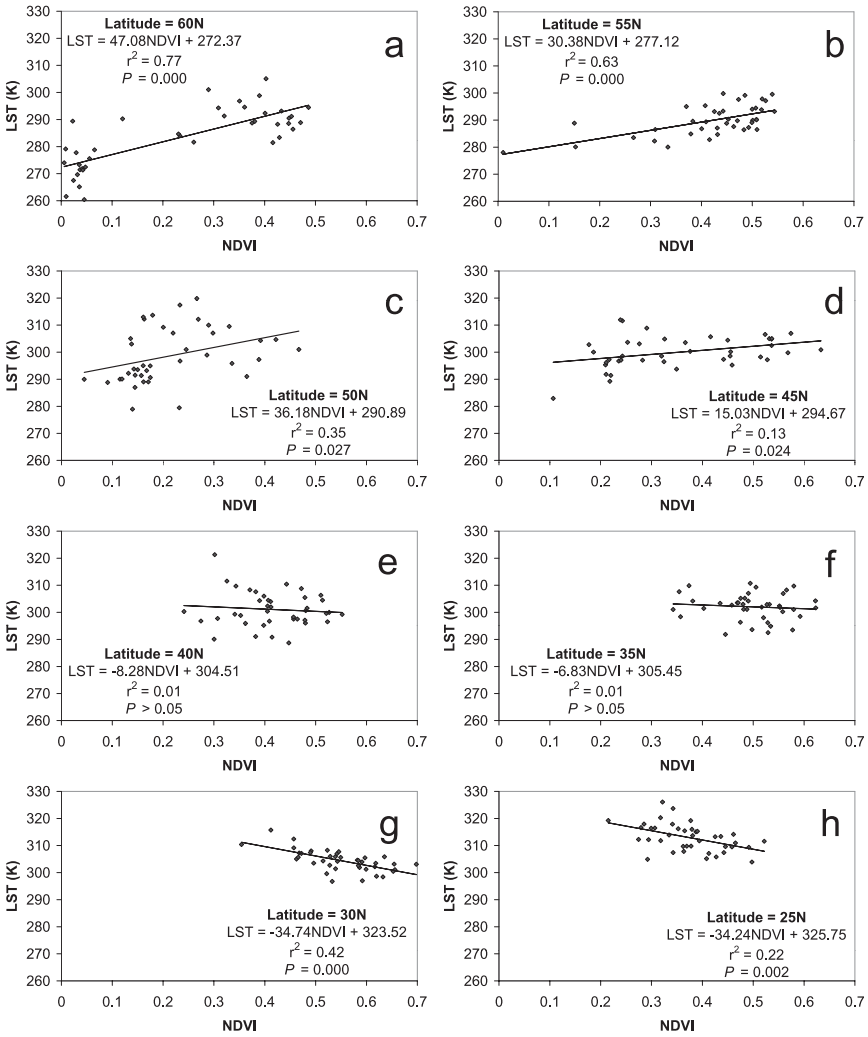

FIG. 3. LST–NDVI correlations at 5° increments along north–south transects from (g) 25°N to (a) 60°N. Note the gradual change of the slope from negative to positive proceeding north.

precipitation can be expected to play a major role during the summer season. The spatiotemporal distributions of these variables are depicted in Fig. 5. To identify which of these climatic factors are most strongly related to spatial distributions of r in different seasons, a multiple linear regression was performed for each subperiod, with r as the dependent variable, and solar radiation, air temperature, and precipitation, each averaged over long-term periods, as independent variables. The regression results are summarized in Table 1.

Additionally, correlation coefficients derived from simple linear regression between r, the three primary climatic variables, and a set of secondary biophysical variables (fractional vegetation cover, soil moisture at the uppermost 10 cm, mean soil moisture at 0–200 cm, and evapotranspiration) are listed in Table 2 to highlight interrelations between these various factors. The β values in Table 2 are the standardized regression coefficients (having variances of 1), allowing comparisons of the magnitude of variation in r explained by each dependent variable.

The total explained variance (coefficient of determination R^2) resulting from the multiple regression is 0.69, 0.51, and 0.61, for the beginning, middle, and end of the growing season subperiods, respectively. Solar radiation appears to be the most dominant driver for the LST–NDVI correlation at the beginning and at the end of the growing season. Analysis of the β coefficients (Table 1) reveals that radiation has the strongest effect on r during the beginning and the end of the growing season ($\beta = -0.57$ and -0.62, respectively), followed by air temperature ($\beta = -0.33$ and -0.17, respectively), and precipitation ($\beta = 0.16$ and 0.08, respectively), with the effects of radiation being more pronounced during the

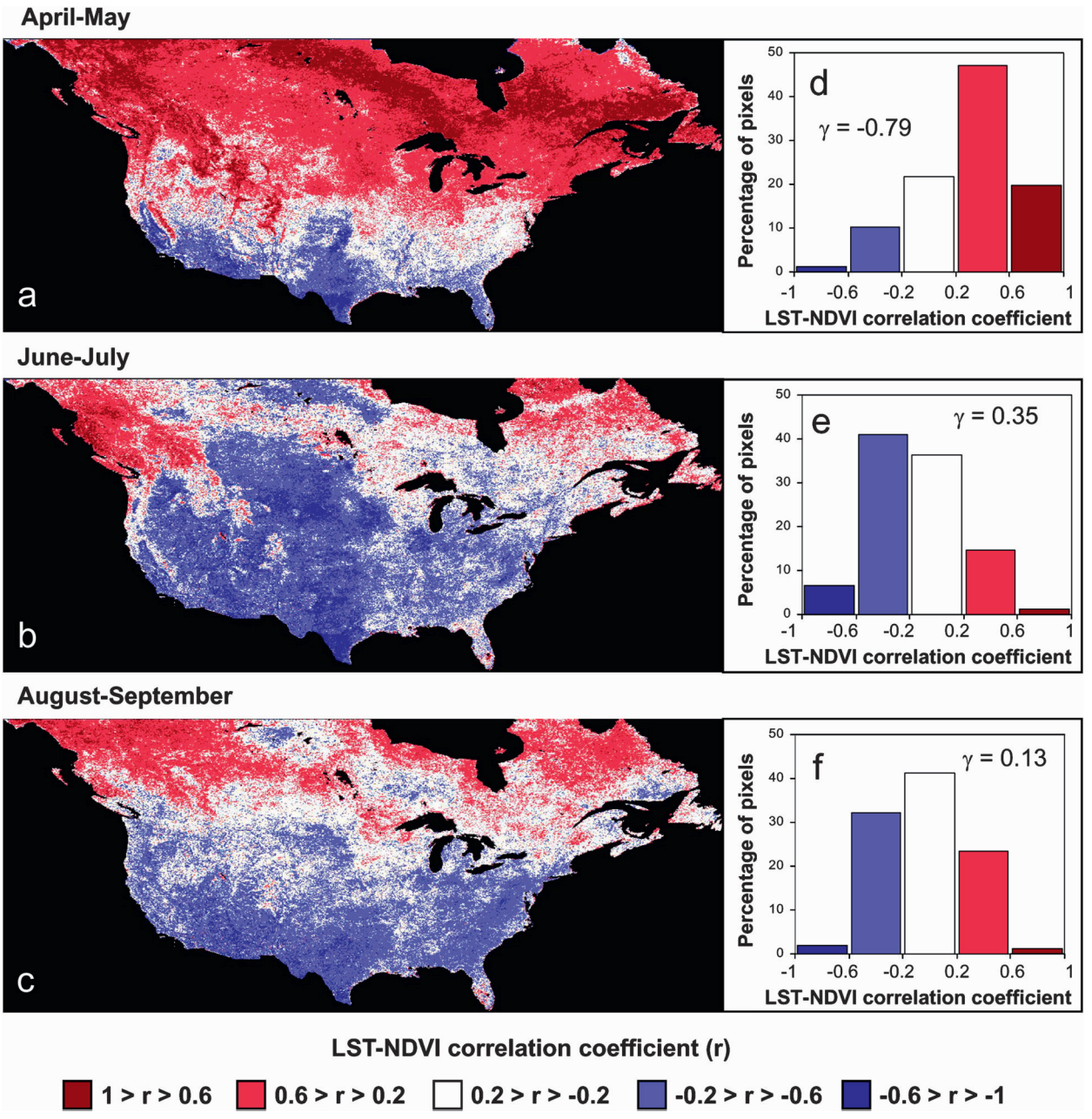

FIG. 4. Spatial distribution of pixels with positive ($r > 0.2$), negative ($r < -0.2$), or insignificant ($-0.2 < r > 0.2$) correlations for the (a)–(c) three subperiods of the growing seasons and (d)–(f) their respective frequency histograms. Histograms and γ values show that at the beginning of the growing season, the majority of the area was characterized by positive correlation; at the middle of the growing season by negative correlation; and at the end of the season by a weaker, yet statistically significant, correlation.

August–September subperiod. Note that for both radiation and air temperature, β has negative values—that is, r decreases as radiation and air temperature increase. The strong dependence of the correlation coefficient on radiation in spring and fall supports the hypothesis that the slope of the LST–NDVI relationship (positive versus negative) reflects the dominant-growth-limiting condition. Where solar radiation and air temperature are typically low (energy-limited conditions), higher LST [reflecting warmer monthly conditions, or lower cloud cover and therefore higher intercepted photosynthetically active radiation (PAR)] is associated with an increase in biomass production, and therefore a positive correlation is expected in these regions.

During the midsummer season (June–July), air temperature explains most of the variance in r ($\beta = -0.76$),

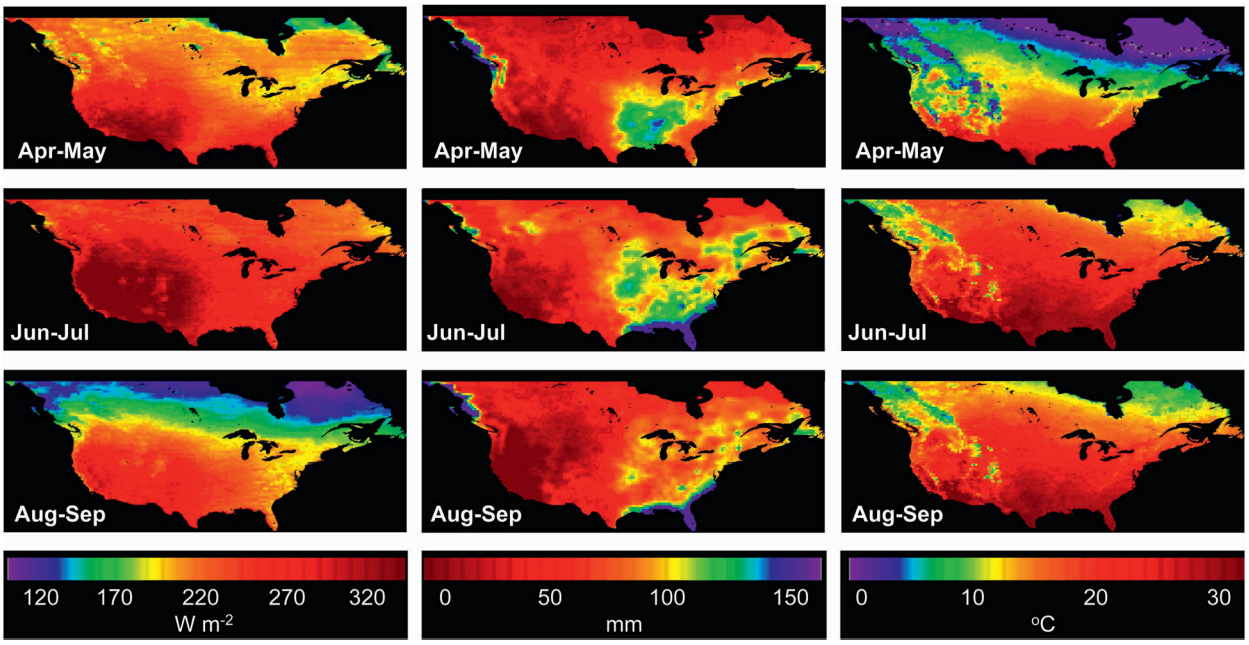

FIG. 5. Spatial distribution of (left) solar radiation, (middle) precipitation, and (right) air temperature over the study area in three subperiods of the growing season.

followed by precipitation ($\beta = 0.23$), with radiation contributing the least ($\beta = 0.07$). Because of the inclination angle of the Earth, the radiation level throughout the entire study area is higher during this period, and even in the northernmost part of the study area, radiation is most likely not a limiting factor for vegetation growth. This is also reflected in the map of correlation coefficient for June–July (Fig. 4b), where, in contrast to the other subperiods, the spatial distribution of r is not strongly stratified by latitude. Cooler air temperatures in Fig. 5 in the northeast and northwest portions of the domain, as well as in the Rockies (as a result of elevation), correlate with areas of positive r, indicative of thermal limits on vegetation growth. Although the radiation map does not correlate with the map of r, the east–west gradient in precipitation across the United States corresponds to similar gradients in r (Figs. 4, 5 for June–July), with low precipitation (moisture-limited growth) areas in the western United States showing the strongest negative correlations between LST and NDVI. Note that in June–July, the overall variance explained by air temperature, radiation, and precipitation is lower than in the other two subperiods (Table 1). This suggests that when radiation is limiting plant growth, it strongly affects the LST–NDVI relationship, whereas under non-radiation-limiting conditions, the nature of LST–NDVI correlations is more complex and not easily explained by simple linear relationships.

Multiple regressions were also performed with the full set of biophysical variables listed in Table 2. Note that whereas solar radiation, precipitation, and air temperature are primary driving forces in the soil–biosphere–atmosphere system, these biophysical variables reflect the response of the system to climatic forcings. Including

TABLE 1. Results of multiple regressions between r (dependent variable) and the driving (independent) variables—precipitation (Precip), radiation (Rad), and air temperature—performed separately for each of the three subperiods. The regression coefficient is B, and β values are the standardized regression coefficients (having variances of 1). Std err is standard error.

	Model	Precip	Rad	Air temperature
Apr–May				
R^2	0.689			
Std err	0.195			
B		0.0018	−0.0088	−0.0167
Significance	$P < 0.0000$	$P < 0.00$	$P < 0.00$	$P < 0.00$
β		0.16	−0.57	−0.33
Jun–Jul				
R^2	0.507			
Std err	0.228			
B		0.0023	0.0010	−0.0430
Significance	$P < 0.0000$	$P < 0.00$	$P < 0.00$	$P < 0.00$
β		0.23	0.07	−0.76
Aug–Sep				
R^2	0.605			
Std err	0.195			
B		0.0008	−0.0054	−0.0088
Significance	$P < 0.0000$	$P < 0.00$	$P < 0.00$	$P < 0.00$
β		0.08	−0.62	−0.17

TABLE 2. Mean and standard deviation (STD) of variables examined for influence on the LST–NDVI relationship and the correlation coefficient matrix for each of the three subperiods. The following notations are used: Tair (air temperature at 2 m); fc (fractional vegetation cover); SM_10 (soil moisture at the uppermost 10 cm); SM_200 (mean soil moisture at 0–200 cm); and ET (evapotranspiration). VF stands for volumetric fraction. All correlations are highly significant ($P < 0.001$).

	Means	STD	r (–)	Precip (mm day^{-1})	Rad (W m^{-2})	Tair (°C)	fc (–)	SM_10 (VF)	SM_200 (VF)	ET (Kg m^{-2})
Apr–May										
r	0.29	0.35	1							
Precip	55.65	32.12	−0.14	1						
Rad	224.85	22.71	−0.80	0.32	1					
Tair	8.73	6.91	−0.76	0.35	0.85	1				
fc	0.32	0.16	−0.23	0.60	0.39	0.51	1			
SM_10	0.25	0.06	−0.02	0.51	0.16	0.28	0.58	1		
SM_200	0.23	0.08	−0.25	0.54	0.44	0.45	0.56	0.88	1	
ET	0.27	0.13	−0.33	0.75	0.50	0.58	0.83	0.70	0.69	1
Jun–Jul										
r	−0.15	0.32	1							
Precip	71.94	31.93	0.13	1						
Rad	255.97	24.79	−0.55	−0.11	1					
Tair	18.62	5.77	−0.68	0.12	0.78	1				
fc	0.50	0.17	0.20	0.54	−0.30	−0.14	1			
SM_10	0.23	0.05	0.39	0.45	−0.24	−0.31	0.43	1		
SM_200	0.24	0.05	0.21	0.18	0.08	−0.13	0.25	0.75	1	
ET	0.41	0.16	0.02	0.67	−0.03	0.13	0.81	0.52	0.39	1
Aug–Sep										
r	−0.05	0.31	1							
Precip	64.05	31.24	0.09	1						
Rad	206.14	35.68	−0.77	−0.01	1					
Tair	17.01	5.98	−0.72	−0.05	0.89					
fc	0.50	0.18	0.24	0.50	−0.21	−0.26	1			
SM_10	0.22	0.05	0.27	0.48	−0.25	−0.36	0.41	1		
SM_200	0.22	0.05	0.16	0.31	−0.14	−0.28	0.08	0.73	1	
ET	0.26	0.11	−0.13	0.64	0.24	0.15	0.74	0.48	0.18	1

all eight variables in the analysis resulted in a similar ranking of the three primary factors, explaining the overall variance in *r*.

c. *Relationship with land cover*

Another biophysical variable that may influence the temporal relationship between LST and NDVI is land cover type. Figure 6 presents the spatial distribution of six main land cover types over the study area, which were also mentioned in section 2c(3). Inclusion of these land cover classes as dummy variables in the multiple regression analyses (similar to the analyses described earlier) confirms that their contribution is statistically significant, although the addition to the total explained variance is small (data not shown). Nevertheless, analysis of the role land cover plays in the distribution of *r* is worthwhile.

Table 3 presents the percent area of the land cover classes that correspond to negative ($r < -0.2$), insignificant ($-0.2 < r < 0.2$), and positive ($r > 0.2$) correlations between LST and NDVI over the entire domain during the three subperiods. Spatial agreement between areas of significant *r* and different land cover classes may be visually observed by comparing Figs. 4a–c, 6 for each of the subperiods, respectively. Several examples are highlighted here. In April–May, 80% of the area of evergreen needleleaf forest shows a correlation between NDVI and LST. This class is clearly apparent in Fig. 4a, including forest patches in the Rockies and the Sierra Nevada. The deciduous broadleaf forests of the Appalachians, on the other hand, show insignificant LST–NDVI correlations (white in Fig. 4a). These forests are located at lower elevations than those in the west and consequently are more susceptible to moisture-limiting conditions than to temperature limits, whereas moisture stress in the low-lying coastal forests in the Pacific Northwest is less prevalent. These results are in agreement with a study by Churkina and Running (1998), who demonstrated that vegetation growth in 74% of the evergreen needleleaf forest, globally distributed, is limited by temperature, whereas growth in 64% of deciduous broadleaf forests are limited by water availability. Olthof and Latifovic (2007) examined the short-term response of vegetation NDVI to LST in Canada and reported that

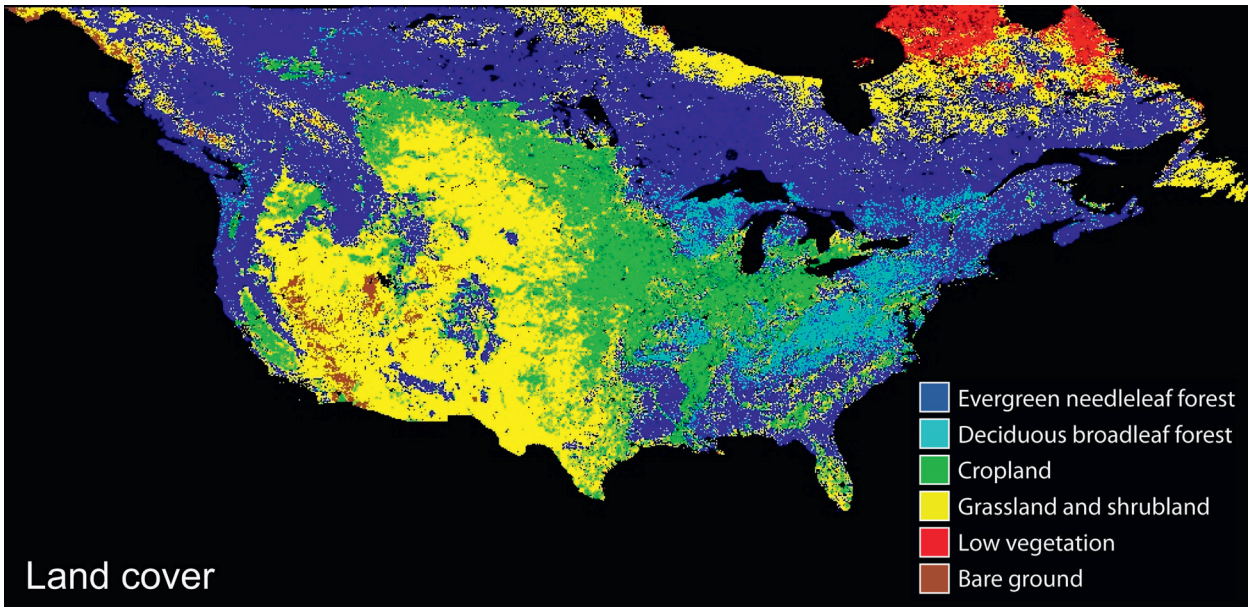

FIG. 6. Spatial distribution of six land cover types aggregated from the land cover classification map generated by the Department of Geography, University of Maryland (Hansen et al. 2000).

several land cover types (namely, trees and shrubs) also exhibit a significant increase in NDVI with higher-than-normal temperatures. In these areas, the VHI may produce false signals of vegetation stress.

During June–July, the mid-growing season, the majority of the cropland areas (80%), along with the grassland and shrubland (68%) and bare ground (55%) in the Southwest (SW) and the Great Plains are characterized by strong negative correlations between LST and NDVI. Similarly, according to Churkina and Running (1998), 99% of the growth of C4 grassland and 95% of the desert shrubland are controlled by water availability. These findings suggest that the VHI can be effectively applied to the agricultural areas of North America during the midsummer season. During this season, 52% of the evergreen needleleaf forested areas, including the forest patches in the Rockies and the Sierra Nevada (SN), tend to exhibit insignificant correlation and 80% of the low vegetation in northeast Canada corresponds to positive *r*.

In August–September, visual correlations between *r* and the land cover classes are less obvious. The low-vegetation class (e.g., tundra) in northern Canada shows the strongest spatial correspondence with *r*, with 77% of this class associated with positive correlations between LST and NDVI. In addition, grassland and shrubland in Canada are characterized by positive values of *r*. The needleleaf forests, however, show mixed trends, with the majority of this class (44%) showing insignificant NDVI–LST correlations. Cropland, and grassland and shrubland classes are almost evenly divided between negative (44% and 46%, respectively) and insignificant (48% and 37%) correlations.

The dry season in Florida (FL) extends from November to April, whereas precipitation in May through October is enhanced because of thunderstorms and tropical disturbances (Fig. 5). A corresponding transition moisture-limited (negative *r*) conditions to energy-limited (positive *r*) conditions can be observed in Florida between the April–May and June–July subperiods (Fig. 4). In most of Texas, Arizona, and southern California, the negative LST–NDVI correlation holds during the entire growing season. In contrast, most of the territory of British Colombia and northern Quebec is characterized by a permanent positive correlation. Correlations between LST and NDVI tend to be less significant along the Mississippi River basin, where irrigation and shallow water tables ameliorate moisture limitations to plant growth even during the midsummer.

4. Summary and conclusions

This paper explores the spatial and temporal relationship between LST and NDVI over the North American continent during the summer growing season (April–September) in the context of its utility for drought monitoring. In contrast to the common perception that LST and NDVI are typically negatively correlated, we demonstrate that this relationship in fact varies with location, season, and vegetation type. Many attempts have been made to interpret this relationship in terms of

TABLE 3. Percent of domain area showing negative ($r < -0.2$), insignificant ($-0.2 < r < 0.2$), and positive ($r > 0.2$) correlations between LST and NDVI during the three subperiods.

	Percent area		
	$r < -0.2$	$-0.2 < r < 0.2$	$r > 0.2$
Apr–May			
Evergreen needleleaf forest	5	15	80
Deciduous broadleaf forest	4	46	50
Cropland	15	28	57
Grassland and shrubland	20	28	52
Low vegetation	7	24	68
Bare ground	32	39	29
Total	15	25	60
Jun–Jul			
Evergreen needleleaf forest	29	52	19
Deciduous broadleaf forest	46	49	4
Cropland	80	19	1
Grassland and shrubland	68	20	12
Low vegetation	0	20	80
Bare ground	55	16	29
Total	57	29	14
Aug–Sep			
Evergreen needleleaf forest	24	44	32
Deciduous broadleaf forest	51	40	9
Cropland	44	48	9
Grassland and shrubland	46	37	17
Low vegetation	1	22	77
Bare ground	49	21	30
Total	38	40	22

various biophysical and geographical variables (e.g., land use and land cover, fractional vegetation cover, moisture conditions, topography). This study revealed that during the beginning and the end of the growing season, solar radiation is the predominant factor driving the correlation between LST and NDVI, whereas other biophysical variables play a lesser role. This behavior has often been missed in earlier studies of more limited scope, typically conducted over the central United States during the growing season.

It was found that when energy is the limiting factor for vegetation growth, as is the case at higher latitudes and elevations in the study area, a positive correlation exists between LST and NDVI. Conversely, during the midseason, the radiative flux over most of the study area is high enough not to limit vegetation growth, and solar radiation plays a smaller role in determining the nature of the LST–NDVI correlation. During this subperiod, except for the northernmost areas, the LST–NDVI correlations are generally negative.

Because droughts occur mostly in low latitudes, several vegetation health and drought indices (e.g., the LST–NDVI ratio and the VHI) were developed based on the assumption that a strong negative correlation between NDVI and LST exists. In such areas, water is ultimately the limiting factor for vegetation growth throughout the year, making this assumption correct. Subsequently, however, these indices have been applied globally with the implicit assumption that NDVI and LST are always and everywhere negatively correlated. On the bases of the current study, there is a need to reexamine this assumption and restrict applications of such an approach to areas and periods where negative correlations are observed.

It is concluded that spaceborne monitoring of vegetation health and droughts based on empirical LST–NDVI relationships is valid for much of the United States during the middle of the growing season, but utility is more limited in the spring and fall and at higher latitudes. Similar and complementary research should be conducted over other continents to assess the global distribution of the LST–NDVI relationship and its temporal variation. Global–annual assessments of the VHI and other related indices should be used with caution. An alternative approach for monitoring vegetation health might be to incorporate understanding of the important driving physical variables and their effect on NDVI and LST, for example, through physically based surface energy balance models (Anderson et al. 2007).

Acknowledgments. We wish to thank the NASA Headquarters' Land Cover Land Use Change Program, the NASA Goddard Space Flight Center, and the University of Maryland's Earth System Science Interdisciplinary Center (ESSIC) for support (Grant NNG04GM89G). NARR data were obtained from NOAA/OAR/ESRL PSD, Boulder, Colorado, from their Web site at http://www.cdc.noaa.gov/. The work that led to the availability of the radiative fluxes was supported by NASA EOD/IDS Grant NAG59634 and by Grant NNG04GD65G from the Radiation Sciences Program, Earth Science Division, Science Mission Directorate. The ISCCP data were obtained from the NASA Langley Research Center Atmospheric Sciences Data Center. Finally, the authors wish to thank the anonymous reviewers for their important and constructive comments.

REFERENCES

Achard, F., and F. Blasco, 1990: Analysis of vegetation seasonal evolution and mapping of forest cover in West Africa with the use of NOAA AVHRR HRPT data. *Photogramm. Eng. Remote Sens.,* **56,** 1359–1365.

Anderson, M. C., J. M. Norman, J. R. Mecikalski, J. A. Otkin, and W. P. Kustas, 2007: A climatological study of evapotranspiration and moisture stress across the continental United States based on thermal remote sensing: 1. Model formulation. *J. Geophys. Res.,* **112,** D10117, doi:10.1029/2006JD007506.

Badeck, F. W., A. Bondeau, K. Bottcher, D. Doktor, W. Lucht, J. Schaber, and S. Sitch, 2004: Responses of spring phenology to climate change. *New Phytol.,* **162,** 295–309.

Boegh, E., H. Soegaard, N. Hanan, P. Kabat, and L. Lesch, 1999: A remote sensing study of the NDVI-T_s relationship and the transpiration from sparse vegetation in the Sahel based on high-resolution satellite data – An overview. *Remote Sens. Environ.,* **69,** 224–240.

Boken, V. K., G. Hoogenboom, F. N. Kogan, J. E. Hook, D. L. Thomas, and K. A. Harrison, 2004: Potential of using NOAA-AVHRR data for estimating irrigated area to help solve an inter-state water dispute. *Int. J. Remote Sens.,* **25,** 2277–2286.

Carlson, T. N., R. R. Gillies, and E. M. Perry, 1994: A method to make use of thermal infrared temperature and NDVI measurements to infer soil water content and fractional vegetation cover. *Remote Sens. Rev.,* **52,** 45–59.

Chapin, F. S., G. R. Shaver, A. E. Giblin, K. J. Nadelhoffer, and J. A. Laundre, 1995: Responses of Arctic Tundra to Experimental and Observed Changes in Climate. *Ecology,* **76,** 694–711.

Choudhury, B. J., N. U. Ahmed, S. B. Idso, R. J. Reginato, and C. S. T. Daughtry, 1994: Relations between evaporation coefficients and vegetation indices studied by model simulations. *Remote Sens. Environ.,* **50,** 1–17.

Churkina, G., and S. W. Running, 1998: Contrasting climatic controls on the estimated productivity of global terrestrial biomes. *Ecosystems,* **1,** 206–215.

Coll, C., V. Casselles, J. A. Sobrino, and E. Valor, 1994: On the atmospheric dependence of the split-window equation for land surface temperature. *Int. J. Remote Sens.,* **15,** 105–122.

Dall'Olmo, G., and A. Karnieli, 2002: Monitoring phenological cycles of desert ecosystems using NDVI and LST data derived from NOAA-AVHRR imagery. *Int. J. Remote Sens.,* **23,** 4055–4071.

Defries, R. S., M. C. Hansen, and J. R. G. Townshend, 2000: Global continuous fields of vegetation characteristics: A linear mixture model applied to multi-year 8 km AVHRR data. *Int. J. Remote Sens.,* **21,** 1389–1414.

Dormann, C. F., and S. J. Woodin, 2002: Climate change in the Arctic: Using plant functional types in a meta-analysis of field experiments. *Funct. Ecol.,* **16,** 4–17.

Ehrlich, D., and E. F. Lambin, 1996: Broad scale land-cover classification and interannual climatic variability. *Int. J. Remote Sens.,* **17,** 845–862.

Ek, M. B., K. E. Mitchell, Y. Lin, E. Rogers, P. Grunmann, V. Koren, G. Gayno, and J. D. Tarpley, 2003: Implementation of Noah land surface model advances in the National Centers for Environmental Prediction operational mesoscale Eta model. *J. Geophys. Res.,* **108,** 8851, doi:10.1029/2002JD003296.

Friedl, M. A., and F. W. Davis, 1994: Sources of variation in radiometric surface-temperature over a Tallgrass Prairie. *Remote Sens. Environ.,* **48,** 1–17.

Gillies, R. R., and T. N. Carlson, 1995: Thermal remote sensing of surface soil water content with partial vegetation cover for incorporation into climate models. *J. Appl. Meteor.,* **34,** 745–756.

——, ——, J. Cui, W. P. Kustas, and K. S. Humes, 1997: A verification of the 'triangle' method for obtaining surface soil water content and energy fluxes from remote measurements of the Normalized Difference Vegetation Index (NDVI) and surface radiant temperature. *Int. J. Remote Sens.,* **18,** 3145–3166.

Gitelson, A. A., F. Kogan, E. Zakarin, L. Spivak, and L. Lebed, 1998: Using AVHRR data for quantitive estimation of vegetation conditions: Calibration and validation. *Adv. Space Res.,* **22,** 673–676.

Goetz, S. J., 1997: Multi-sensor analysis of NDVI, surface temperature and biophysical variables at a mixed grassland site. *Int. J. Remote Sens.,* **18,** 71–94.

Goward, S. N., and A. S. Hope, 1989: Evapotranspiration from combined reflected solar and emitted terrestrial radiation: Preliminary FIFE results from AVHRR data. *Adv. Space Res.,* **9,** 239–249.

——, G. D. Cruickshanks, and A. S. Hope, 1985: Observed relation between thermal emission and reflected spectral radiance of a complex vegetated landscape. *Remote Sens. Environ.,* **18,** 137–146.

——, R. H. Waring, D. G. Dye, and J. L. Yang, 1994: Ecological remote sensing at OTTER: Satellite macroscale observations. *Ecol. Appl.,* **4,** 322–343.

——, Y. Xue, and K. P. Czajkowski, 2002: Evaluating land surface moisture conditions from the remotely sensed temperature/vegetation index measurements: An exploration with the simplified simple biosphere model. *Remote Sens. Environ.,* **79,** 225–242.

Graglia, E., S. Jonasson, A. Michelsen, and I. K. Schmidt, 1997: Effects of shading, nutrient application and warming on leaf growth and shoot densities of dwarf shrubs in two arctic-alpine plant communities. *Ecoscience,* **4,** 191–198.

Gupta, R. K., T. S. Prasad, and D. Vijayan, 2002: Estimation of roughness length and sensible heat flux from WiFS and NOAA AVHRR data. *Land Surface Characterization and Remote Sensing of Ocean Processes,* R. K. Gupta, R. P. Singh, and Y. Menard, Eds., Pergamon Press, 33–38.

Gurney, R. J., J. P. Ormsby, and D. K. Hall, 1983: Observed relation between thermal emission and reflected spectral radiance of a complex vegetated landscape. *Permafrost: Fourth Int. Conf.,* Fairbanks, AK, University of Alaska and National Academy of Sciences, 401–404.

Gutman, G. G., 1990: Towards monitoring droughts from space. *J. Climate,* **3,** 282–295.

Hansen, M. C., R. S. Defries, J. R. G. Townshend, and R. Sohlberg, 2000: Global land cover classification at 1 km spatial resolution using a classification tree approach. *Int. J. Remote Sens.,* **21,** 1331–1364.

Heim, R. R., 2002: A review of twentieth-century drought indices used in the United States. *Bull. Amer. Meteor. Soc.,* **83,** 1149–1165.

Hope, A. S., 1988: Estimation of wheat canopy resistance using combined remotely sensed spectral reflectance and thermal observations. *Remote Sens. Environ.,* **24,** 369–383.

——, and T. P. McDowell, 1992: The relationship between surface temperature and a spectral vegetation index of a tallgrass prairie: Effects of burning and other landscape controls. *Int. J. Remote Sens.,* **13,** 2849–2863.

——, D. E. Petzold, S. N. Goward, and R. M. Ragan, 1986: Simulated relationships between spectral reflectance, thermal emissions, and evapotranspiration of a soybean canopy. *Water Resour. Bull.,* **22,** 1011–1019.

——, S. N. Goward, and D. E. Petzold, 1988: Tersail: A numerical model for combined analysis of vegetation canopy bidirectional reflectance and thermal emissions. *Remote Sens. Environ.,* **26,** 287–300.

Huete, A. R., R. D. Jackson, and D. F. Post, 1985: Spectral response of a plant canopy with different soil backgrounds. *Remote Sens. Environ.,* **17,** 37–53.

Jang, J. D., A. A. Viau, and F. Anctil, 2006: Thermal-water stress index from satellite images. *Int. J. Remote Sens.,* **27,** 1619–1639.

Ji, L., and A. J. Peters, 2003: Assessing vegetation response to drought in the northern Great Plains using vegetation and drought indices. *Remote Sens. Environ.,* **87,** 85–98.

Julien, Y., and J. A. Sobrino, 2009: The Yearly Land Cover Dynamics (YLCD) method: An analysis of global vegetation from NDVI and LST parameters. *Remote Sens. Environ.,* **113,** 329–334.

——, ——, and W. Verhoef, 2006: Changes in land surface temperatures and NDVI values over Europe between 1982 and 1999. *Remote Sens. Environ.,* **103,** 43–55.

Karnieli, A., and G. Dall'Olmo, 2003: Remote-sensing monitoring of desertification, phenology, and droughts. *Manage. Environ. Qual.,* **14,** 22–38.

——, M. Bayasgalan, Y. Bayarjargal, N. Agam, S. Khudulmur, and C. J. Tucker, 2006: Comments on the use of the vegetation health index over Mongolia. *Int. J. Remote Sens.,* **27,** 2017–2024.

Kawashima, S., 1994: Relation between vegetation, surface temperature, and surface composition in the Tokyo region during winter. *Remote Sens. Environ.,* **50,** 52–60.

Kogan, F. N., 1995: Application of vegetation index and brightness temperature for drought detection. *Adv. Space Res.,* **15,** 91–100.

——, 1997: Global drought watch from space. *Bull. Amer. Meteor. Soc.,* **78,** 621–636.

——, 2000: Satellite-observed sensitivity of world land ecosystems to El Nino/La Nina. *Remote Sens. Environ.,* **74,** 445–462.

——, 2002: World droughts in the new millennium from AVHRR-based vegetation health indices. *Eos, Trans. Amer. Geophys. Union,* **83,** 557–564.

Lambin, E. F., 1996: Change detection at multiple temporal scales: Seasonal and annual variations in landscape variables. *Photogramm. Eng. Remote Sens.,* **62,** 931–938.

——, 1997: Land-cover changes in sub-Saharan Africa (1982-1991): Application of a change index based on remotely sensed surface temperature and vegetation indices at a continental scale. *Remote Sens. Environ.,* **61,** 181–200.

——, and A. H. Strahler, 1994a: Change-vector analysis in multitemporal space: A tool to detect and categorize land-cover change processes using high temporal-resolution satellite data. *Remote Sens. Environ.,* **48,** 231–244.

——, and ——, 1994b: Indicators of land-cover change for change-vector analysis in multitemporal space at coarse spatial scales. *Int. J. Remote Sens.,* **15,** 2099–2119.

——, and D. Ehrlich, 1995: Combining vegetation indexes and surface temperature for land-cover mapping at broad spatial scales. *Int. J. Remote Sens.,* **16,** 573–579.

——, and ——, 1996: The surface temperature-vegetation index space for land cover and land-cover change analysis. *Int. J. Remote Sens.,* **17,** 463–487.

——, and ——, 1997: Land-cover changes in sub-Saharan Africa (1982-1991): Application of a change index based on remotely sensed surface temperature and vegetation indices at a continental scale. *Remote Sens. Environ.,* **61,** 181–200.

Liu, H. Q., and R. T. Pinker, 2008: Radiative fluxes from satellites: Focus on aerosols. *J. Geophys. Res.,* **113,** D08208, doi:10.1029/2007JD008736.

——, ——, and B. N. Holben, 2005: A global view of aerosols from merged transport models, satellite, and ground observations. *J. Geophys. Res.,* **110,** D10S15, doi:10.1029/2004JD004695.

——, ——, M. Chin, B. Holben, and L. Remer, 2008: Synthesis of information on aerosol optical properties. *J. Geophys.Res.,* **113,** D07206, doi:10.1029/2007JD008735.

Liu, W. T., and F. N. Kogan, 1996: Monitoring regional drought using the Vegetation Condition Index. *Int. J. Remote Sens.,* **17,** 2761–2782.

McVicar, T. R., and P. N. Bierwirth, 2001: Rapidly assessing the 1997 drought in Papua New Guinea using composite AVHRR imagery. *Int. J. Remote Sens.,* **22,** 2109–2128.

Mesinger, F., and Coauthors, 2006: North American regional reanalysis. *Bull. Amer. Meteor. Soc.,* **87,** 343.

Moran, M. S., T. R. Clarke, Y. Inoue, and A. Vidal, 1994: Estimating crop water deficit using the relation between surface-air temperature and spectral vegetation index. *Remote Sens. Environ.,* **49,** 246–263.

——, A. F. Rahman, J. C. Washburne, D. C. Goodrich, M. A. Weltz, and W. P. Kustas, 1996: Combining the Penman-Monteith equation with measurements of surface temperature and reflectance to estimate evaporation rates of semiarid grassland. *Agric. For. Meteor.,* **80,** 87–109.

Nadelhoffer, K. J., A. E. Giblin, G. R. Shaver, and J. A. Laundre, 1991: Effects of temperature and substrate quality on element mineralization in six Arctic soils. *Ecology,* **72,** 242–253.

Narasimhan, B., R. Srinivasan, and A. D. Whittaker, 2003: Estimation of potential evapotranspiration from NOAA-AVHRR satellite. *Appl. Eng. Agric.,* **19,** 309–318.

Nemani, R., and S. Running, 1989: Estimation of regional surface resistance to evapotranspiration from NDVI and thermal-IR AVHRR data. *J. Appl. Meteor.,* **28,** 276–284.

——, and ——, 1997: Land cover characterization using multitemporal red, near-IR, and thermal-IR data from NOAA/AVHRR. *Ecol. Appl.,* **7,** 79–90.

——, L. Pierce, S. Running, and S. Goward, 1993: Developing satellite-derived estimates of surface moisture status. *J. Appl. Meteor.,* **32,** 548–557.

——, C. D. Keeling, H. Hashimoto, W. M. Jolly, S. C. Piper, C. J. Tucker, R. B. Myneni, and S. Running, 2003: Climate-driven increases in global terrestrial net primary production from 1982 to 1999. *Science,* **300,** 1560–1563.

Olthof, I., and R. Latifovic, 2007: Short-term response of arctic vegetation NDVI to temperature anomalies. *Int. J. Remote Sens.,* **28,** 4823–4840.

Ottle, C., and D. Vidalmadjar, 1994: Assimilation of soil moisture inferred from infrared remote sensing in a hydrological model over the HAPEX-Mobilhy region. *J. Hydrol.,* **158,** 241–264.

Pinker, R. T., and J. A. Ewing, 1985: Modeling surface solar radiation: Model formulation and validation. *J. Climate Appl. Meteor.,* **24,** 389–401.

——, and I. Laszlo, 1992: Modeling surface solar irradiance for satellite applications on a global scale. *J. Appl. Meteor.,* **31,** 194–211.

Price, J. C., 1990: Using spatial context in satellite data to infer regional scale evapotranspiration. *IEEE Trans. Geosci. Remote Sens.,* **28,** 940–948.

Prihodko, L., and S. N. Goward, 1997: Estimation of air temperature from remotely sensed surface observations. *Remote Sens. Environ.,* **60,** 335–346.

Quiring, S. M., and T. N. Papakryiakou, 2003: An evaluation of agricultural drought indices for the Canadian prairies. *Agric. For. Meteor.,* **118,** 49–62.

Rodriguez-Puebla, C., R. T. Pinker, and S. Nigam, 2008: Relationship between downwelling surface shortwave radiative fluxes and sea surface temperature over the tropical Pacific: AMIP II models versus satellite estimates. *Ann. Geophys.,* **26,** 785–794.

Rossow, W. B., and R. A. Schiffer, 1999: Advances in understanding clouds from ISCCP. *Bull. Amer. Meteor. Soc.,* **80,** 2261–2287.

——, and E. N. Dueñas, 2004: The International Satellite Cloud Climatology Project (ISCCP) Web site: An online resource for research. *Bull. Amer. Meteor. Soc.,* **85,** 167–172.

Sandholt, I., K. Rasmussen, and J. Andersen, 2002: A simple interpretation of the surface temperature/vegetation index space for assessment of surface moisture status. *Remote Sens. Environ.,* **79,** 213–224.

Schiffer, R. A., and W. B. Rossow, 1985: ISCCP global radiance data set: A new resource for climate research. *Bull. Amer. Meteor. Soc.,* **66,** 1498–1505.

Schultz, P. A., and M. S. Halpert, 1995: Global analysis of the relationships among a vegetation index, precipitation and land-surface temperature. *Int. J. Remote Sens.,* **16,** 2755–2777.

Seiler, R. A., F. Kogan, and J. Sullivan, 1998: AVHRR-based vegetation and temperature condition indices for drought detection in Argentina. *Adv. Space Res.,* **21,** 481–484.

Smith, R. C. G., and B. J. Choudhury, 1991: Analysis of normalized difference and surface temperature observations over southeastern Australia. *Int. J. Remote Sens.,* **12,** 2021–2044.

Sobrino, J. A., and N. Raissouni, 2000: Toward remote sensing methods for land cover dynamic monitoring: Application to Morocco. *Int. J. Remote Sens.,* **21,** 353–366.

——, M. H. El Kharraz, J. Cuenca, and N. Raissouni, 1998: Thermal inertia mapping from NOAA-AVHRR data. *Adv. Space Res.,* **22,** 655–667.

Stisen, S., I. Sandholt, A. Nørgaard, R. Fensholt, and L. Eklundh, 2007: Estimation of diurnal air temperature using MSG SEVIRI data in West Africa. *Remote Sens. Environ.,* **110,** 262–274.

Stow, D. A., and Coauthors, 2004: Remote sensing of vegetation and land-cover change in Arctic tundra ecosystems. *Remote Sens. Environ.,* **89,** 281–308.

Sui, C. H., X. F. Li, M. M. Rienecker, K. M. Lau, I. Laszlo, and R. T. Pinker, 2003: The role of daily surface forcing in the upper ocean over the tropical Pacific: A numerical study. *J. Climate,* **16,** 756–766.

Sun, D., and M. Kafatos, 2007: Note on the NDVI-LST relationship and the use of temperature-related drought indices over North America. *Geophys. Res. Lett.,* **34,** L24406, doi:10.1029/2007GL031485.

Tateishi, R., and M. Ebata, 2004: Analysis of phenological change patterns using 1982-2000 Advanced Very High Resolution Radiometer (AVHRR) data. *Int. J. Remote Sens.,* **25,** 2287–2300.

Tucker, C. J., 1979: Red and photographic infrared linear combinations for monitoring vegetation. *Remote Sens. Environ.,* **8,** 127–150.

——, and B. J. Choudhury, 1987: Satellite remote sensing of drought conditions. *Remote Sens. Environ.,* **23,** 243–251.

Unganai, L. S., and F. N. Kogan, 1998: Southern Africa's recent droughts from space. *Adv. Space Res.,* **21,** 507–511.

Van Wijk, M. T., M. Williams, J. A. Laundre, and G. R. Shaver, 2003: Interannual variability of plant phenology in tussock tundra: Modelling interactions of plant productivity, plant phenology, snowmelt and soil thaw. *Global Change Biol.,* **9,** 743–758.

Walker, M. D., and Coauthors, 2006: Plant community responses to experimental warming across the tundra biome. *Proc. Natl. Acad. Sci. USA,* **103,** 1342–1346.

Wan, Z., P. Wang, and X. Li, 2004: Using MODIS Land Surface Temperature and Normalized Difference Vegetation Index products for monitoring drought in the southern Great Plains, USA. *Int. J. Remote Sens.,* **25,** 61–72.

Wilhite, D. A., and M. H. Glantz, 1985: Understanding the drought phenomenon: The role of definitions. *Water Int.,* **10,** 111–120.

Zhang, B. L., R. T. Pinker, and P. W. Stackhouse, 2007: An empirical orthogonal function iteration approach for obtaining homogeneous radiative fluxes from satellite observations. *J. Appl. Meteor. Climatol.,* **46,** 435–444.